Spindle assembly checkpoint satisfaction occurs via end-on but not lateral attachments under tension

Jonathan Kuhn[1,2] and Sophie Dumont[1,2,3]

[1]Tetrad Graduate Program, [2]Department of Cell and Tissue Biology, and [3]Department of Cell and Molecular Pharmacology, University of California, San Francisco, San Francisco, CA

To ensure accurate chromosome segregation, the spindle assembly checkpoint (SAC) prevents anaphase until all kinetochores attach to the spindle. What signals the SAC monitors remains unclear. We do not know the contributions of different microtubule attachment features or tension from biorientation to SAC satisfaction nor how these possible cues change during attachment. In this study, we quantify concurrent Mad1 intensity and report on SAC silencing, real-time attachment geometry, occupancy, and tension at individual mammalian kinetochores. We show that Mad1 loss from the kinetochore is switch-like with robust kinetics and that tension across sister kinetochores is established just before Mad1 loss events at the first sister. We demonstrate that CenpE-mediated lateral attachment of the second sister can persistently generate this metaphase-like tension before biorientation, likely stabilizing sister end-on attachment, yet cannot induce Mad1 loss from that kinetochore. Instead, Mad1 loss begins after several end-on microtubules attach. Thus, end-on attachment provides geometry-specific molecular cues or force on specific kinetochore linkages that other attachment geometries cannot provide.

Introduction

The spindle assembly checkpoint (SAC) ensures correct partitioning of the genome (Musacchio and Salmon, 2007; London and Biggins, 2014b) by preventing the onset of anaphase until all sister kinetochores are attached to the spindle (Rieder et al., 1995). The level of SAC proteins at kinetochores regulates cell cycle progression (Collin et al., 2013; Dick and Gerlich, 2013; Heinrich et al., 2013). Specifically, the removal of Mad1 from attached kinetochores controls the anaphase inhibitory signal (Maldonado and Kapoor, 2011). Both tension from biorientation (McIntosh, 1991) and microtubule attachment have been proposed to control Mad1 loss from kinetochores in mammalian cells (Pinsky and Biggins, 2005; Etemad and Kops, 2016). Although tension across the centromere is not essential for SAC satisfaction (Rieder et al., 1995; O'Connell et al., 2008), tension within (and across) a single kinetochore may be (Maresca and Salmon, 2009; Uchida et al., 2009). Across which linkages tension could be monitored and whether that tension would be necessary, sufficient, or neither remain unclear (Etemad et al., 2015; Tauchman et al., 2015; Magidson et al., 2016; Smith et al., 2016). Instead, or in addition, the SAC may monitor the presence of microtubules or specific attachment features, such as whether the kinetochore binds to the end (end-on) or side (lateral) of microtubules (i.e., geometry), how many microtubules it binds (occupancy), and the timescale over which it remains attached to any—or a given—microtubule (lifetime).

We do not know what physical changes ultimately trigger Mad1 loss and, critically, we do not know how changes in tension and attachment features map to those of Mad1 at individual kinetochores during mammalian spindle assembly. One barrier is that to this point we have only visualized tension, attachment, and SAC signaling together in fixed cells. Challenges to live imaging these dynamics include concurrently visualizing individual kinetochores moving in 3D, dim microtubule structures, and dim Mad1, as well as doing so at high resolution over long periods. Because tension and attachment candidate cues both evolve during mitosis (McEwen et al., 1997; Magidson et al., 2011) and often covary and go through short-lived intermediates, uncoupling their contributions has been difficult. In particular, it is not yet clear whether lateral attachments, which use motors rather than Ndc80 for binding microtubules, are able to trigger SAC silencing (Cheeseman and Desai, 2008; Nezi and Musacchio, 2009; Kops and Shah, 2012), nor whether the answer to this is based on the specificity of their molecular interface or on a different stability or force-generating ability. Determining which kinetochore interfaces can and cannot trigger SAC silencing upon binding to or being pulled on by microtubules is essential to understanding what the kinetochore monitors in order to control cell cycle progression.

In this study, we develop an approach to quantitatively map in real time the structural dynamics of centromere tension,

Correspondence to Sophie Dumont: Sophie.Dumont@ucsf.edu

Abbreviations used: SAC, spindle assembly checkpoint; SKAP, small kinetochore-associated protein; STLC, S-trityl-L-cysteine.

The Rockefeller University Press $30.00
J. Cell Biol. Vol. 216 No. 6 1533–1542
https://doi.org/10.1083/jcb.201611104

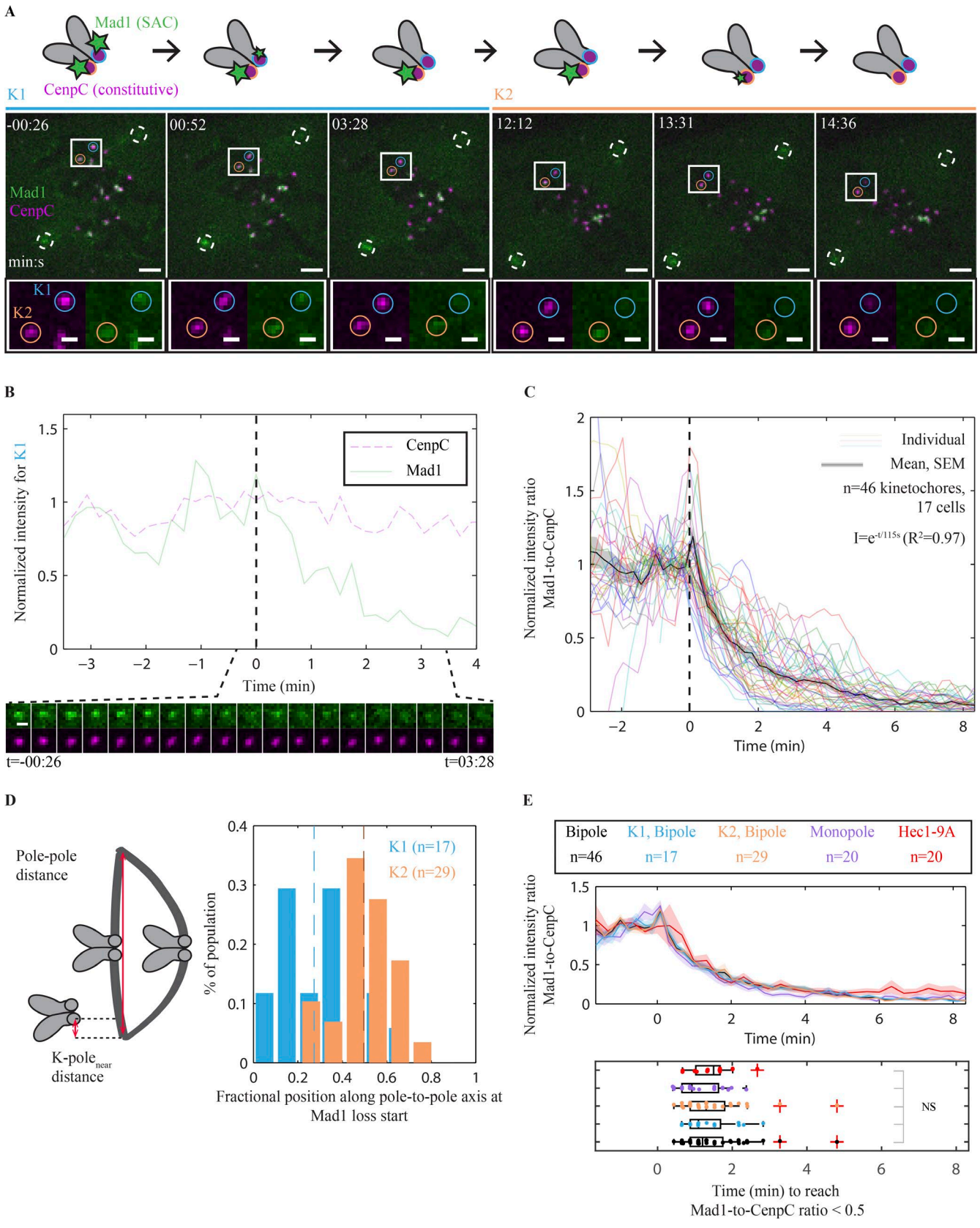

Figure 1. **Mad1 loss at individual mammalian kinetochores is a switch-like process with robust stereotypical single exponential kinetics.** (A) Time-lapse imaging (maximum-intensity projections) of representative SAC satisfaction kinetics (EYFP-Mad1; green) at individual kinetochores (CenpC-mCherry; magenta) during spindle assembly in a PtK2 cell. Full circles identify the first (K1; blue) and second (K2; orange) sisters in a pair to lose Mad1, and white dashed circles identify spindle poles. $t = 0$ indicates the start of Mad1 loss on K1. See also Video 1. (B) Mad1 (solid green) and CenpC (dashed magenta) intensities for K1 in panel A around SAC satisfaction. Time lapse (bottom) of K1 at 13-s intervals. Bars: (A, main images) 3 µm; (A, insets, and B) 1 µm.

attachment geometry, and attachment occupancy onto those of Mad1 signaling at individual mammalian kinetochores during spindle assembly. Collectively, our work reveals the space–time trajectory of a sister pair to SAC silencing and indicates that engagement of microtubule ends is the trigger for SAC silencing. We demonstrate that CenpE-based lateral attachments can generate long-lived force and are thus well suited to stabilize end-on attachments before biorientation, but they cannot satisfy the SAC. Thus, end-on attachment must provide specific molecular cues or force on a specific linkage to control the SAC that other persistent, force-generating attachments cannot provide.

Results and discussion

To measure the real-time kinetics of Mad1 depletion once initiated at individual kinetochores, we used a two-color reporter consisting of EYFP-Mad1 and CenpC-mCherry (Fig. 1 A). Mad1 localization is necessary and sufficient for SAC activation (Maldonado and Kapoor, 2011), its N- or C-terminal EYFP fusions behave similarly (Shah et al., 2004), and Mad1 binding and dissociation kinetics are well understood on unattached (but not on attached) kinetochores (Howell et al., 2004; Shah et al., 2004; Dick and Gerlich, 2013). In turn, CenpC is a stable kinetochore component (Shah et al., 2004). The ratio of Mad1 to CenpC intensities controls for variations in kinetochore size and for out-of-focal-plane movements. We imaged this reporter live over four focal planes with ∼10 s resolution in mammalian PtK2 cells. These cells are ideal for tracking kinetochores and mapping physical attachment and tension changes as they are large, flat, and have few chromosomes. We tracked individual kinetochores from prophase or prometaphase to metaphase using CenpC-mCherry and then quantified reporter intensities (Fig. 1 A).

We found that Mad1 levels at individual kinetochores are stable during spindle assembly (Mad1-ON state) until they drop sharply to background (Mad1-OFF state), whereas CenpC levels stay constant (Fig. 1, A and B; and Video 1). Although there may be short-lived fluctuations in Mad1 levels that we cannot detect, we did not find intermediate steady states with intensities between those of Mad1-ON and -OFF states, and we did not observe any significant rerecruitment of Mad1 upon the completion of Mad1 loss. To determine the distribution of Mad1 loss rates, we aligned all Mad1 loss events in time at the start of Mad1 loss ($t = 0$). This revealed that Mad1 loss kinetics are switch-like and strikingly similar over kinetochores and cells ($n = 46$ kinetochores in 17 cells; Fig. 1 C). The kinetics of Mad1 loss are well fit by a single exponential ($t_{1/2} = 79$ s; $R^2 = 0.97$; Fig. 1 C), with only a marginal fit improvement with a double exponential ($R^2 = 0.99$). This suggests that the process of removing Mad1 from kinetochores has one rate-limiting step. This single event could, for example, be the turnover of phosphorylation marks involved in recruiting Mad1 (Nijenhuis et al., 2014) or Mad1 removal by dynein (Howell et al., 2001).

To probe the events that govern Mad1 loss, we examined Mad1 removal at individual kinetochore pairs and in different conditions. Mad1 loss events at each sister were broadly distributed in time (10.6 ± 9.5 min apart; Fig. S1 A), and thus pairs with a single SAC-satisfying sister exist (Gorbsky and Ricketts, 1993) and are broadly distributed in space (Figs. 1 D and S1 B). Although this distribution in space does not have a large effect on the distribution in time (Fig. S1 C), it follows a particular pattern: the first sister in a pair to satisfy the SAC began losing Mad1 close to its spindle pole, often as it transitioned from poleward to away-from-pole movement; meanwhile, the second sister began losing Mad1 at a different location ($P = 0.0001$), close to the metaphase plate and typically after a sharp movement toward the plate that also aligned (Magidson et al., 2015) sisters along the pole-to-pole axis (Fig. S1 D). Despite these differences, Mad1 loss events at the first and second kinetochores had indistinguishable kinetics after the onset of Mad1 loss (Fig. 1 E). We then asked what physical properties of the kinetochore, if any, regulated this rate-limiting step in Mad1 loss (Pinsky and Biggins, 2005). We hypothesized that tension or attachment, both proposed to be required for Mad1 loss, tune kinetics of Mad1 removal after its onset. To test this hypothesis, we imaged Mad1 in cells with monopolar spindles (Fig. S2, A and B), which have lower tension (Fig. S2 D), and in cells expressing Hec1-9A–mRuby2 (Fig. S2 C), which have higher tension (Fig. S2 D) and microtubule occupancy (Zaytsev et al., 2014). We used centromere stretch (interkinetochore [K–K] distance) as a reporter of tension; although centromere stretch is not itself necessary for SAC satisfaction, changes in centromere stretch imply changes in load on the kinetochore fiber (k-fiber) and across at least some kinetochore linkages. Despite these tension differences, Mad1 loss kinetics remained unchanged in monopoles ($P = 0.12$; $n = 20$ kinetochores; Fig. 1 E and Video 2) and Hec1-9A cells ($P = 0.35$; $n = 20$ kinetochores; Fig. 1 E). This suggests that after the onset of Mad1 loss, the rate of loss is insensitive to tension and attachment occupancy levels; once the SAC satisfaction decision is made, the kinetochore silences the SAC in a stereotypical event.

To gain insight into what events initiate Mad1 loss, we quantified how tension and attachment change before and around these stereotypical Mad1 loss events. We began by measuring the K–K distance of a sister pair before and during Mad1 loss (Fig. 2, A–C; and Video 3). In all cases mapped, the K–K distance of a single chromosome increased just before the first sister lost Mad1 (Fig. 2, B and C): it started at 1.06 ± 0.06 µm for $t < -2$ min, indistinguishable ($P = 0.64$) from that in nocodazole ($n = 10$ pairs), and increased ($P = 0.001$) to 2.14 ± 0.32 µm by $t = 0$, the start of Mad1 loss (Fig. 2 D). The K–K distance as Mad1 left the first kinetochore was higher in bipoles than in monopoles (2.14 ± 0.32 µm vs. 1.20 ± 0.03;

(C) Individual traces, means, and SEM of the Mad1/CenpC intensity ratio (I) over time (t) around SAC satisfaction with traces synchronized at $t = 0$ ($n = 46$ kinetochores). (D) Distribution of the fractional position along the pole-to-pole axis ((k-pole$_{near}$)/(pole–pole)) where kinetochores start to lose Mad1. Dashed lines indicate the mean position for each sister. The first sister (K1; $n = 17$) loses Mad1 close to its pole, and the second sister (K2; $n = 29$) near the metaphase plate. (E) Mean and SEM (top) of the Mad1/CenpC intensity ratio with $t = 0$ Mad1 loss start, and distribution (bottom) of times to reach a threshold intensity ratio, in bipolar cells ($n = 46$ kinetochores), different kinetochores (K1 and K2; $n = 17$ and 29) in these cells, in monopolar spindles (STLC-treated; Video 2; $n = 20$ kinetochores) that have lower tension, and in Hec1-9A–expressing cells, which have higher tension and attachment levels ($n = 20$ kinetochores). Vertical lines on box plots indicate the minimum value (except outliers), 25th percentile, median value, 75th percentile, and maximum value (except outliers). Red crosses indicate outlier values >1.5× the interquartile range. In all cases, Mad1 loss kinetics are indistinguishable from controls (NS; $P > 0.05$; two-sided Mann-Whitney U test).

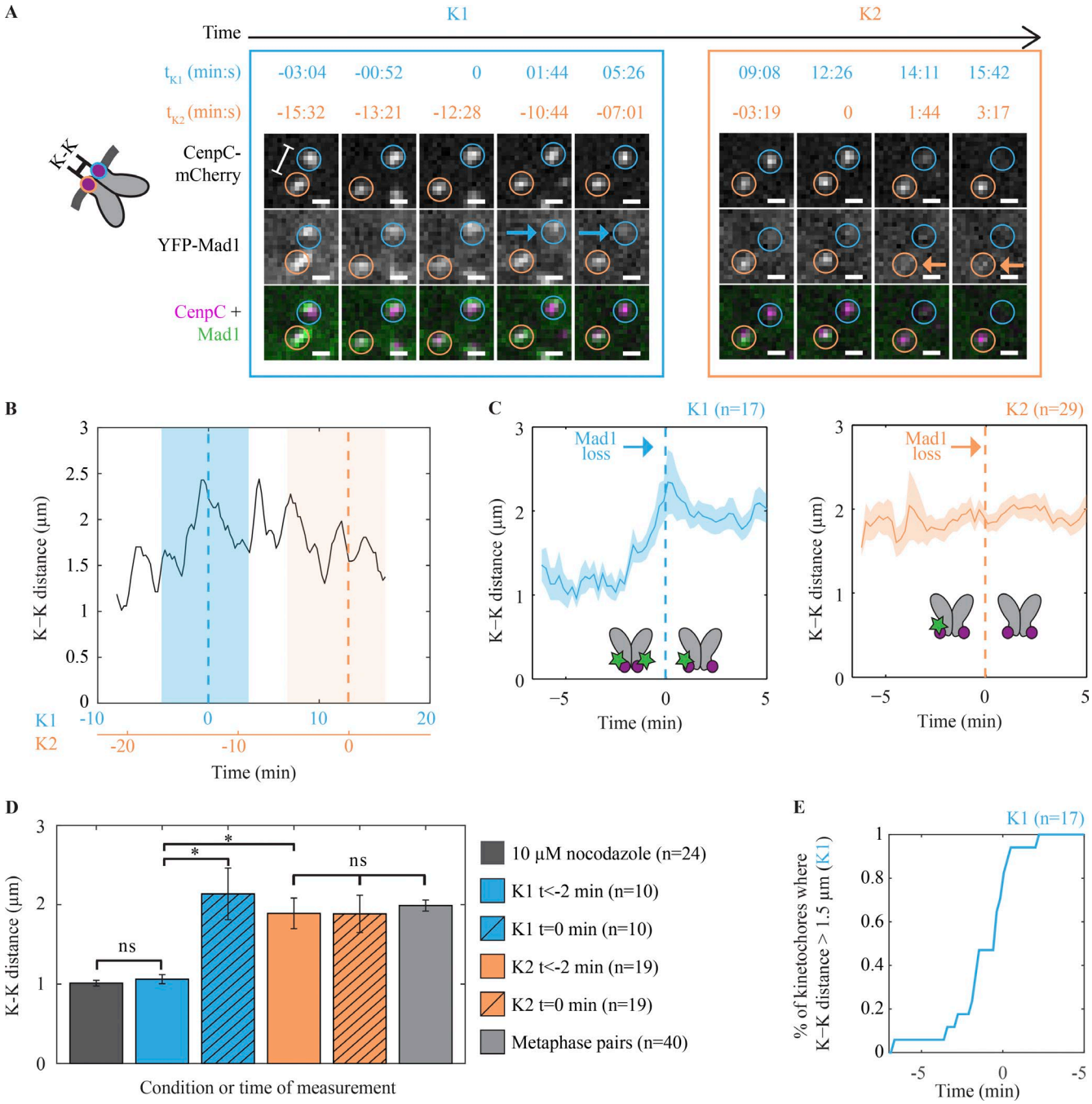

Figure 2. **Kinetochores are under metaphase-level tension before Mad1 loss, but tension across the kinetochore is insufficient to initiate Mad1 loss.** (A) Time-lapse imaging (maximum-intensity projection) of SAC satisfaction kinetics (EYFP-Mad1) concurrently with K–K distance (CenpC-mCherry) showing representative changes in centromere tension (ruler) relative to Mad1 loss (start at $t = 0$, followed by arrows) on K1 (blue) and K2 (orange) from the PtK2 cell in Fig. 1 A. See also Video 3. Bars, 1 µm. (B) K–K distance over time for the pair in A with smoothing over a three-time-point window and $t = 0$ (dashed lines) indicating the start of Mad1 loss for K1 (blue) and K2 (orange). (C) Means and SEM of K–K distance over time plotted relative to Mad1 loss start ($t = 0$) for each of K1 (left; $n = 17$ pairs) and K2 (right; $n = 29$ pairs). (D) K–K distance at all time points before $t = -2$ min for K1 ($n = 10$ pairs) and K2 ($n = 19$ pairs) at $t = 0$ for K1 ($n = 10$ pairs) and K2 ($n = 19$ pairs) and at reference points in separate experiments (metaphase kinetochores [$n = 40$ pairs] and 10 µM nocodazole [$n = 24$ pairs]). Measurements for K2's $t = -2$ min do not include any data before K1's $t = 0$. Error bars indicate SEM (*, $P < 0.05$; two-sided Mann-Whitney *U* test). (E) Fraction of pairs ($n = 17$) with a K–K distance crossing >1.5 µm as time evolves relative to Mad1 loss start at K1 ($t = 0$).

P = 0.02; Figs. 2 D and S2 D), suggesting that an opposing force other than polar ejection acts before silencing the first kinetochore in normal bipolar mammalian mitosis. The K–K distance increase just before Mad1 loss, in all cases measured (Fig. 2 E), is consistent with (but does not imply) tension across the kinetochore being necessary to initiate Mad1 loss. However, kinetochore pairs persist at a metaphase level of tension (P = 0.10) for minutes without Mad1 loss at the second sister (1.89 ± 0.19 µm for $t < -2$ min; $n = 19$ pairs; Fig. 2 D) with no significant tension increase (P = 0.82) at $t = 0$ (1.89 ± 0.14 µm). Thus, neither microtubule attachment nor the transmission of force (i.e., load bearing) across the kinetochore,

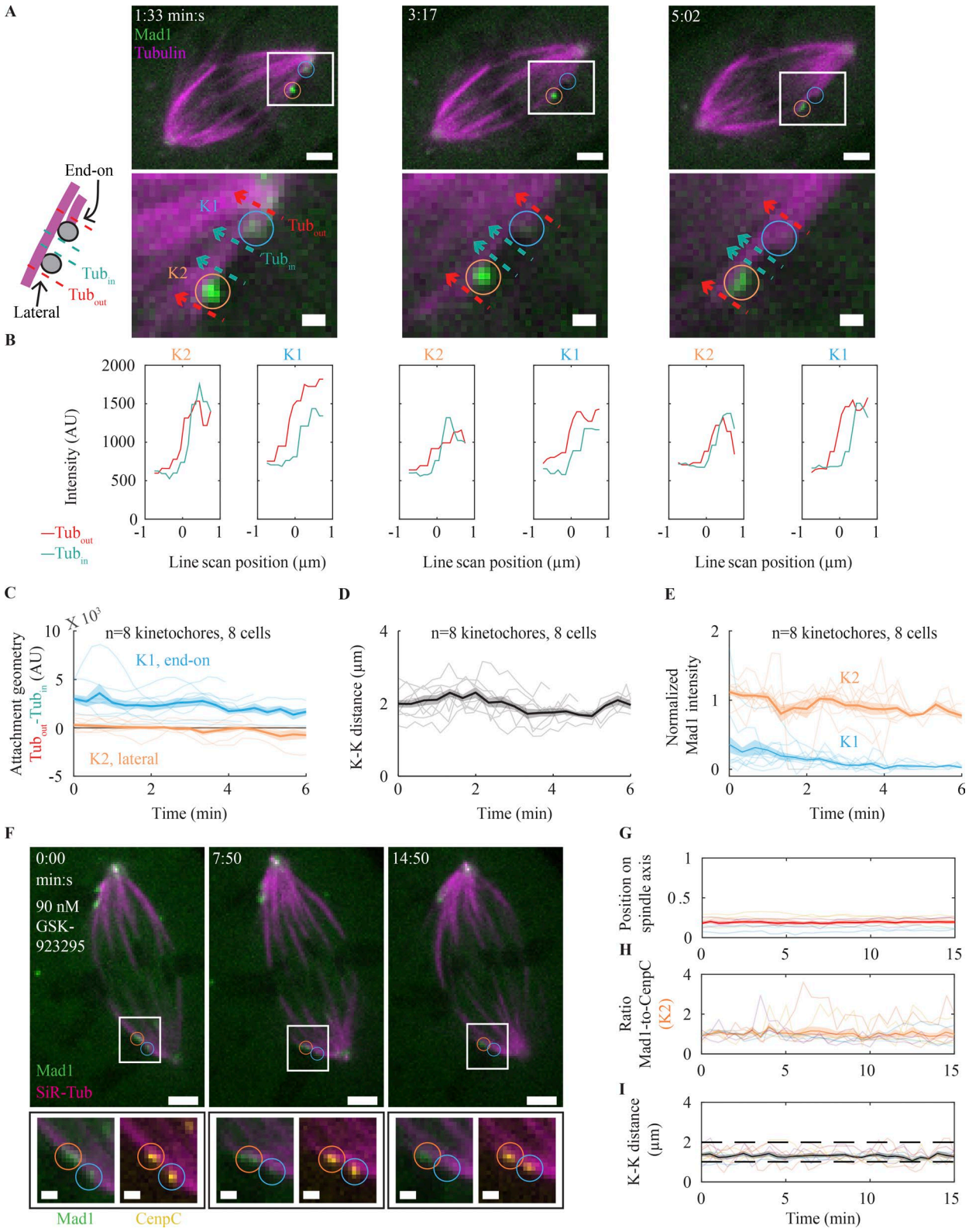

Figure 3. **Lateral attachments generating long-lived metaphase-level centromere tension do not satisfy the SAC.** (A) Time-lapse imaging (maximum-intensity projection) of representative SAC satisfaction kinetics (EYFP-Mad1) and microtubule attachment (mCherry-tubulin) in a PtK2 cell. K2 (orange circle) sits along the side of a neighboring k-fiber, suggesting a lateral attachment, but remains Mad1 positive while its sister K1 (blue circle) loses Mad1. Bottom images display the analysis depicted in B. $t = 0$ indicates video start. See also Video 4. (B) Analysis of microtubule geometry comparing the tubulin intensity (integrated line scans) inside (Tub_{in}) and outside (Tub_{out}) the pair in A. The intensity difference is high on K1, indicating an end-on attachment, and is near zero on K2, indicating a lateral attachment. (C) Individual, mean, and SEM of $Tub_{out} - Tub_{in}$ for K1 (blue) and K2 (orange) in pairs where K2 begins Mad1 positive (n = eight pairs). AU, arbitrary unit. (D) Individual, mean, and SEM of K–K distances for the traces in C (n = eight pairs). (E) Individual, mean, and Mad1 intensity for K1 (end-on; blue) and K2 (lateral; orange) in C and D (n = eight pairs). (F) Time-lapse imaging (maximum-intensity projection) of

from chromosome to microtubule, is sufficient to satisfy the SAC in normal dividing cells.

To uncover how kinetochores form persistent force-generating attachments without satisfying the SAC, we concurrently quantified Mad1 intensity and the position and intensity of microtubules at kinetochores in live cells. We expressed EYFP-Mad1 and mCherry-tubulin (Fig. 3 A and Video 4). On pairs with one Mad1-ON sister (K2; orange), the Mad1-ON sister was associated with a microtubule bundle whose intensity continued past the kinetochore rather than terminating at it (Fig. 3 A and Video 4). This is consistent with motor-driven lateral kinetochore–microtubule attachments, which we identified as cases where (a) the tubulin intensity was equal on both sides of a kinetochore (Fig. 3 B) and (b) where there was centromere tension (Kapoor et al., 2006) confirming productive microtubule engagement. We detected the same intermediates (pairs under tension with one lateral Mad1-ON kinetochore and one Mad1-OFF kinetochore) in fixed PtK2 cells stained for endogenous Mad2 (Fig. S3, A–C; $n = 17$ pairs), validating EYFP-Mad1 as a live-cell reporter. Despite interactions with lateral microtubules (Fig. 3, A–C) and high tension for long periods (Fig. 3 D), the levels of Mad1 on these kinetochores did not change ($n =$ eight kinetochores; Fig. 3 E).

Consistent with the lateral attachments imaged being powered by CenpE, a plus end–directed kinesin, rigor inhibition of this motor with GSK-923295 (Fig. 3 F; Wood et al., 2010) generated kinetochore pairs stuck near a pole that failed to congress (Fig. 3 G). These pairs remained with one laterally attached Mad1-positive sister ($n = 10$ kinetochores; Fig. 3 H and Video 5; Magidson et al., 2015), under some, albeit reduced, centromere tension (Fig. 3 I). Thus, stable lateral microtubule–kinetochore attachments that generate long-lived metaphase centromere tension levels exist during normal mitosis, are mediated by CenpE, and are not sufficient to (even partially) satisfy the SAC. If the SAC monitors tension across the kinetochore, it must do so across a kinetochore linkage that is not put under sufficient load in these lateral attachments.

Finally, to probe how microtubule attachment geometry and occupancy changed before and around Mad1 loss, we imaged three-color cells expressing EYFP-Mad1 and CenpC-mCherry and stained with the far-red microtubule dye SiR-tubulin (Fig. 4 A and Video 6; Lukinavičius et al., 2014). We captured Mad1 loss events for the second kinetochore in a pair and concurrently quantified (Fig. 4, A and B) the dynamics of Mad1 intensity (Fig. 4 C), microtubule attachment geometry and occupancy (Fig. 4 D), and centromere tension (Fig. 4 E) at single kinetochores. Strikingly, signature Mad1 loss events (Fig. 4 C) always coincided with a sharp increase in end-on microtubule occupancy levels ($n = 21$ kinetochores; Fig. 4, B and D). As the first several microtubule ends bind from $t = -100$ s to $t = 0$ ($P = 0.002$; Fig. 4 D), there was no corresponding decrease in Mad1 levels (Fig. 4 C). After several end-on microtubules had bound, which we estimated to be half of a mature k-fiber (and thus ∼10–12 microtubules in PtK cells; McEwen et al., 1997), Mad1 loss then initiated ($t = 0$) before end-on attachment levels reached their mature k-fiber levels at $\sim t = 100$ s ($P = 0.002$). Over this same time period, there was no change in centromere tension on these kinetochores (Fig. 4 E). Consistent with end-on attachments maturing during Mad1 loss, small kinetochore-associated protein (SKAP)–ΔEB-tdTomato, which specifically binds kinetochores with mature attachments (Schmidt et al., 2010), began to localize at kinetochores as EFYP-Mad1 left and apparent end-on attachments (SiR-tubulin) formed ($n = 13$ pairs; Fig. S3 D). Collectively, our work indicates that the trigger for Mad1 loss is kinetochore engagement to microtubule ends and that this engagement provides a unique, geometry-specific cue, whether molecular or physical, that other persistent force-generating attachments cannot provide.

Many elegant studies have used genetic and chemical perturbations to change tension and kinetochore–microtubule attachments and thereby probe the events triggering Mad1 depletion. In this study, our approach was to image naturally occurring centromere tension and attachment changes during spindle assembly as well as to map those to the real-time kinetochore SAC silencing response. This allowed us to map a trajectory of events, which is likely one of a few, leading to SAC satisfaction in unperturbed cells (Fig. 5).

The contributions of tension and attachment (lifetime, geometry, and occupancy) have been hard to decouple. In this study, we identify a long-lived state with high centromere tension and no detectable end-on attachment. Consistently, Mad1 had been found at some laterally attached kinetochores in fixed cells (Dick and Gerlich, 2013; Shrestha and Draviam, 2013; Drpic et al., 2015; Magidson et al., 2015); however, whether the captured attachments were stable and generated sustained force, and therefore whether end-on geometry was the only missing element of a correct attachment, was not known. Although lateral attachments have been proposed to help SAC protein stripping (Howell et al., 2000), and lateral attachments satisfy the SAC in budding yeast (Shimogawa et al., 2010; Krefman et al., 2015), end-on attachment is necessary for SAC satisfaction in mammalian cells. The pathways that control dynein-dependent SAC protein stripping may also help confer end-on geometric specificity (Gassmann et al., 2010; Matson and Stukenberg, 2014) in mammals. Mammalian cells are thought to use both dynein-dependent and -independent pathways for Mad1 removal (Gassmann et al., 2010), and their individual contributions to this process are not yet clear. Finally, what are the minimal attachment events sufficient for SAC satisfaction? We found that Mad1 loss begins without a full complement of microtubules; further, the different kinetics of k-fiber formation and Mad1 loss suggest that there is not simply a linear relationship between them. Mapping the precise relationship between microtubule occupancy and SAC signaling will require tools to disrupt the rapid k-fiber formation (McEwen et al., 1997) that we observed.

In unperturbed mitosis, we never observed Mad1 loss before tension generation. Our data strongly suggest that lateral

representative SAC inactivation kinetics (EYFP-Mad1) and microtubule attachment (SiR-tubulin) at a kinetochore pair (CenpC-mCherry) in a PtK2 cell where some kinetochores are locked in a CenpE-mediated lateral attachment (90 nM GSK-923295 CenpE inhibitor) for >15 min. (A and F) Bars: 3 µm (top); 1 µm (bottom). $t = 0$ indicates video start. See also Video 5. (G–I) Analysis (individual, mean, and SEM) of fractional position along the pole-to-pole axis (G; also see Fig. 1 D), Mad1/CenpC intensity ratio (H), and K–K distance for such K2 kinetochores highlighted in F (I), where $t = 0$ indicates video start ($n =$ 10 kinetochores). Dashed black lines in I indicate reference mean K–K distances (same data as Fig. 2 D) for pairs in nocodazole (bottom; $n = 24$ pairs) and at metaphase (top; $n = 40$ pairs).

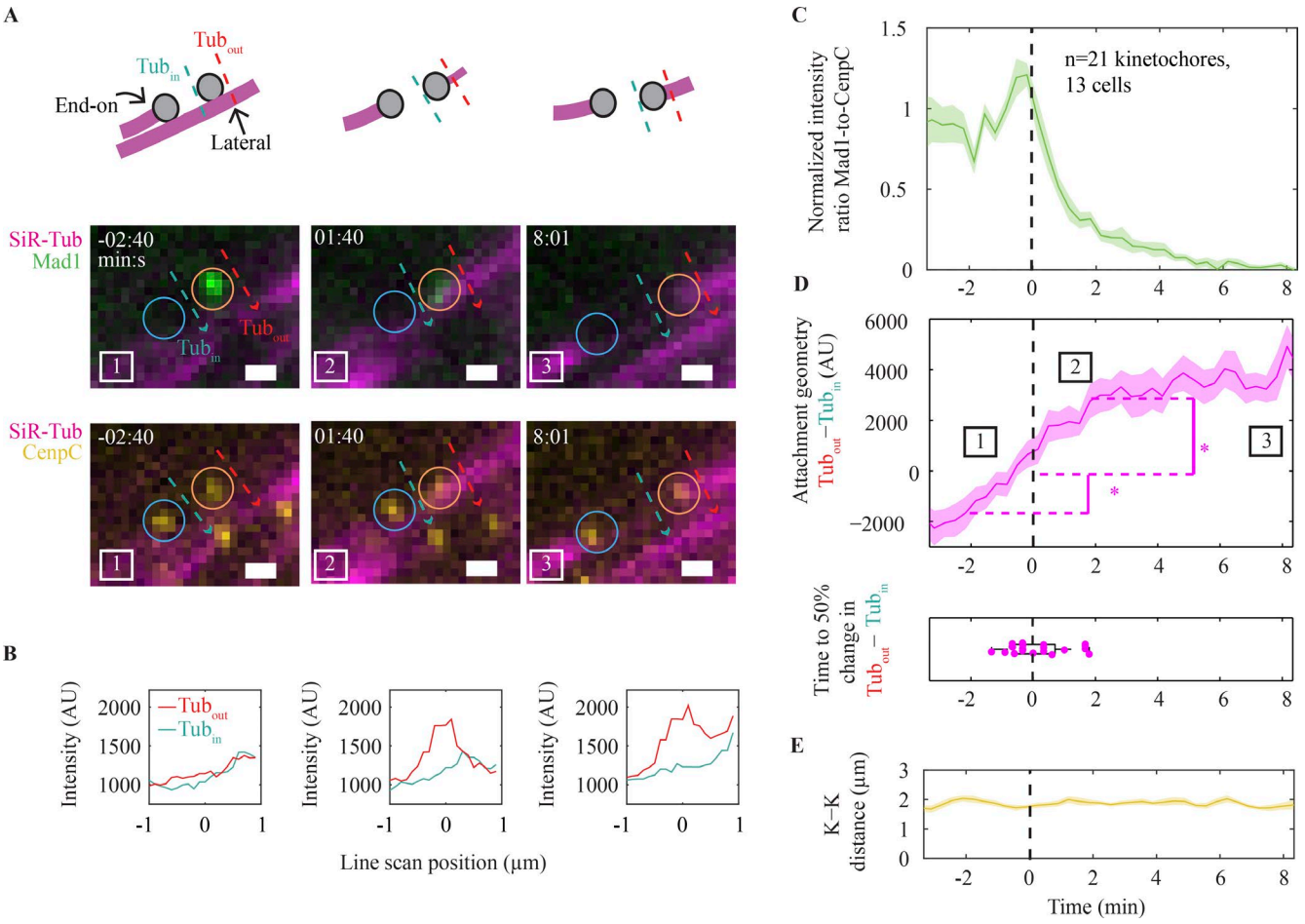

Figure 4. **Mad1 loss begins rapidly after end-on attachment initiation and before a full k-fiber forms.** (A) Time-lapse imaging (maximum-intensity projection) of a representative kinetochore pair's SAC satisfaction kinetics (EYFP-Mad1; Mad1 loss start at $t = 0$), attached microtubules' geometry and intensity (SiR-tubulin), and centromere tension (CenpC-mCherry) in a PtK2 cell. Dashed arrows illustrate analysis shown in B. Bars, 1 µm. See also Video 6. (B) Microtubule attachment geometry (and occupancy) analysis as an end-on attachment forms, corresponding with images in A. A negative value indicates that the kinetochore is near the end of its lateral microtubule track. (C–E) Concurrent quantification (mean and SEM) of the Mad1/CenpC intensity ratio (C), microtubule attachment geometry (Tub_{out}–Tub_{in}; D), and tension (K–K distance) around SAC satisfaction (E), with $t = 0$ indicating the start of Mad1 loss on K2 ($n = 21$ kinetochores). Boxed numbers map to images in A. Mad1 loss starts rapidly after end-on attachment initiation, when less than a full complement of microtubules is bound. *, $P < 0.01$; Wilcoxon signed-rank test. AU, arbitrary unit.

attachments, which may be differently sensitive (Kalantzaki et al., 2015) to destabilization at low tension, facilitate end-on attachment formation by generating tension (King and Nicklas, 2000; Nicklas et al., 2001; Nezi and Musacchio, 2009; Khodjakov and Pines, 2010; Foley and Kapoor, 2013) before biorientation. Although polar ejection forces may generate tension across these kinetochores (Cane et al., 2013; Drpic et al., 2015), higher tension levels may be needed for stabilization. Methods to decouple attachment and tension across the kinetochore will be needed to determine whether the latter is necessary for SAC satisfaction. Critically, the inability of persistent force-generating lateral attachments to satisfy the SAC ensures that only bioriented attachments both stabilize kinetochore–microtubule interactions and satisfy the SAC to control cell cycle progression. The imaging approach we developed, used in different molecular backgrounds and with different fluorescent SAC reporters, should help uncover the cascade of events linking end-on microtubule engagement to SAC satisfaction.

Upon attachment, several mechanisms may confer plus end specificity. For example, the plus end may engage a geometry-specific kinetochore interface because of its unique structure and dynamics, or plus end geometry may allow kinetochore components to engage with more microtubules. Mps1, a kinase upstream of Mad1 localization (London and Biggins, 2014a), is regulated in an end-on–specific manner. Lateral attachments through CenpE may not compete with Mps1 for Ndc80 binding (Hiruma et al., 2015; Ji et al., 2015) or may not access the proper kinetochore interface to pull Mps1 away from its substrates (Aravamudhan et al., 2015). The dynamics of SKAP localization that we observe (Fig. S3 D) suggest a decrease in Aurora B and/or an increase in PP1 activity (Schmidt et al., 2010) once end-on attachments form, consistent with a model where end-on attachment specifically triggers a shift in the phosphorylation state of outer kinetochore substrates.

If tension-based deformations within a kinetochore are important for SAC signaling, our findings suggest that these deformations must be highly specific to end-on microtubule attachments. Furthermore, our work suggests that if tension is sensed, it would likely be sensed at a linkage outside of the junction where CenpE- and Ndc80-based attachments both transmit force (i.e., bear loads) to the centromere (Fig. 5, boxes 1 and 2). Looking forward, it will be important to determine

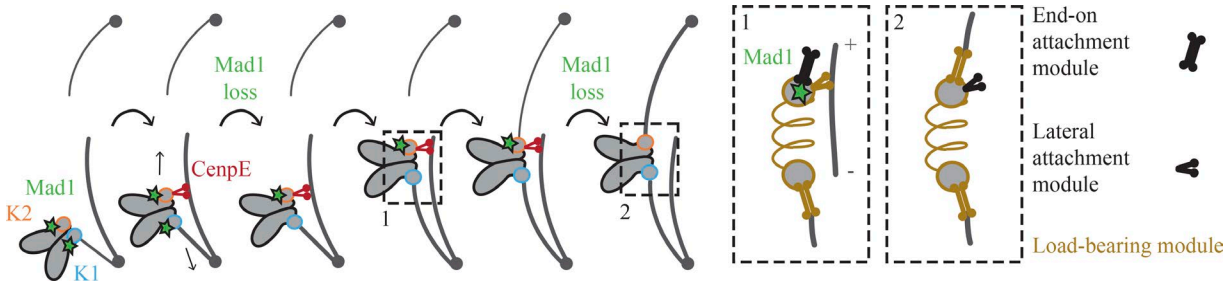

Figure 5. **Model for attachment trajectory and triggering cue leading to SAC silencing of sister kinetochores.** In the trajectory we mapped, the first kinetochore (K1; blue circle) lost Mad1 (green star) and satisfied the SAC near its pole. The second kinetochore (K2) laterally attached through CenpE (red motor), generating tension that can stabilize end-on attachment of K1, thereby helping K1 bypass tension-based inhibition of initial end-on attachments. Despite being able to transmit force and bear loads from the outer to inner kinetochore (Box 1; gold), this attachment does not induce Mad1 loss at K2. CenpE pulls the pair toward the metaphase plate, where K2 forms end-on microtubule attachments and rapidly loses Mad1. SAC satisfaction must be triggered by a geometry-specific cue unique to an end-on attachment that CenpE-based attachments (even persistent force-generating ones) cannot supply. This cue could, for example, be binding interactions specific to end-on attachments or deformation of a linkage that only bears a sufficient load in an end-on attachment (Box 2; gold).

what kinetochore structural and biochemical changes take place when lateral and end-on attachments form.

Materials and methods

Cell culture and transfection

PtK2 EYFP-Mad1 cells (gifts from J. Shah; Shah et al., 2004) and wild-type PtK2 cells were cultured at 37°C and 5% CO_2 in MEM supplemented with sodium pyruvate (Invitrogen), nonessential amino acids, penicillin/streptomycin, and 10% qualified and heat-inactivated fetal bovine serum as previously described (Elting et al., 2014). For imaging, cells were plated on 35-mm dishes with #1.5 poly-D-lysine–coated coverslips (MatTek Corporation), and media were switched to identical media without phenol red 24 h before imaging. Cells were transfected using Fugene6 or Viafect (Promega) and imaged 36–48 h after transfection with mCherry–α-tubulin (a gift from M. Davidson, Florida State University, Tallahassee, FL), mCherry-CenpC (a gift from A. Straight, Stanford University, Stanford, CA), SKAP-ΔEB-tdTomato (a gift from I. Cheeseman, Massachusetts Institute of Technology and the Whitehead Institute, Cambridge, MA), or Hec1-9A–mRuby2 (mRuby2 [a gift from M. Davidson] was swapped for EGFP in Hec1-9A–EGFP [a gift from J. DeLuca, Colorado State University, Fort Collins, CO; Guimaraes et al., 2008]).

Drug and dye treatments

To make monopolar spindles, 5 µM S-trityl-L-cysteine (STLC; Sigma-Aldrich) was added 15 min before imaging (10 mM stock). To rigor CenpE to microtubules, 90 nM GSK-923295 (MedChem Express) was added 15 min before imaging (30 µM stock; Magidson et al., 2015). To visualize tubulin as a third color, 100 nM SiR-tubulin dye (Cytoskeleton, Inc.) was added 1 h before imaging (1 mM stock) along with 10 µM verapamil (10 mM stock; Cytoskeleton, Inc.) to prevent dye efflux.

Immunofluorescence

For immunofluorescence, cells were fixed in 95% methanol with 5 mM EGTA for 1 min. The following antibodies were used: mouse anti–α-tubulin DM1 (1:1,000; T6199; Sigma-Aldrich), human anti-centromere (CREST; 1:25; 15-234-0001; Antibodies, Inc.), rabbit anti–rat kangaroo-Mad2 (1:100; a gift from J. DeLuca and J. Mick), mouse and rabbit secondary antibodies conjugated to Alexa Fluor 488 and 647, respectively (1:500; A11001 and A21244; Invitrogen), and a human secondary antibody conjugated to DyLight 405 (1:100; 109-475-098; Jackson ImmunoResearch Laboratories, Inc.).

Imaging

Live imaging was performed on an inverted (Eclipse T*i*-E; Nikon) spinning-disk confocal microscope (CSU-X1; Yokogawa Electric Corporation) with a Di01-T405/488/561 head dichroic (Semrock), 488-nm (120 mW) and 561-nm (150 mW) diode lasers, emission filters (ET525/50M or ET630/75M; Chroma Technology Corp.), and an iXon3 camera (Andor Technology) as previously described (Elting et al., 2014) for two-color imaging. For three- and four-color imaging, a Di01-T405/488/568/647 head dichroic (Semrock) was used, along with 405-nm (100 mW) and 642-nm (100 mW) diode lasers and ET455/50M and ET690/50M emission filters (Chroma Technology Corp.). Cells were imaged by phase contrast (200–400-ms exposures) and fluorescence (40–75-ms exposures) in four z planes spaced 350 nm apart every 13–30 s, with a 100× 1.45 Ph3 oil objective through a 1.5× lens (MetaMorph 7.7.8.0; Molecular Devices). All live images were collected at bin = 2 (to improve imaging contrast for dim Mad1 and microtubule structures), 5× preamplifier gain, and no EM gain (210 nm/pixel). Cells were imaged at 30°C and 5% CO_2 with phenol red–free MEM media in a closed, humidity-controlled Tokai Hit PLAM chamber. The only image processing done before display were maximum-intensity projections at each time point and (for videos only) linear scaling up of the image size in ImageJ (National Institutes of Health). Fixed-cell images (Fig. S3, A–C) were acquired 200 nm apart with bin = 1, and images are displayed as sum intensity projections of all frames where the highlighted pair was visible.

Data analysis

Tracking. Kinetochore pairs were visually identified by coordinated motion and selected for analysis if they stayed away from other kinetochores and if at least one sister lost Mad1 during the video. All further analysis was done within MATLAB (MathWorks). If mCherry-CenpC was present, kinetochores were tracked using SpeckleTracker (shared by X. Wan; Wan et al., 2012); if it was not present (Fig. 3), kinetochore tracking was done manually using Mad1, tubulin, and phase-contrast images and custom software. Spindle poles were tracked manually.

Intensity measurements. To measure EYFP-Mad1 and mCherry-CenpC intensities at each time point, videos were thresholded by setting to zero all pixels less than two SDs above image background at the first frame. For each time point, the intensities of all pixels in a 5 × 5 pixel (1.05 × 1.05 µm) box around the kinetochore were summed

together over all planes. The same operation was performed at areas outside the spindle and subtracted from the kinetochore intensity. Time points with no detectable CenpC were not analyzed.

To calculate tubulin intensity around a given kinetochore (Figs. 3 and 4), two intensity line scans (1.5 µm long) were taken perpendicular to the sister kinetochore axis: one positioned 0.7 µm toward the centromere (Tub_{in}) and one 0.7 µm away from the centromere (Tub_{out}). To synchronize traces to the beginning of Mad1 loss, traces were examined visually to locate the time where Mad1 levels dropped while CenpC levels remained constant, and $t = 0$ was set for the time point immediately before such Mad1 loss began. The Mad1/CenpC ratio was then normalized to the mean ratio from −100 to 0 s. In Fig. 3 (E and H; no Mad1 loss), intensities were normalized to K2's Mad1 intensity in the first 100 and 300 s of the trace, respectively. Immunofluorescence intensities were measured on sum intensity projections using a 3-pixel-wide (0.315 µm) line scan for tubulin and a 10 × 10 pixel (1.05 × 1.05 µm) box for Mad2 and CREST.

Other measurements. Kinetochore-to-pole distances (Fig. 1 D) were calculated by projecting where an individual kinetochore fell on the pole-to-pole axis. The "near" pole was designated as the pole closest to K1 at the time of K1's Mad1 loss start.

Statistics. Data are expressed as means ± SEM. Calculations of p-values (Mann-Whitney *U* and Wilcoxon Signed-Rank tests) were done in StatPlus (AnalystSoft).

Online supplemental material

Fig. S1 describes the spatiotemporal trajectory of sister kinetochores around Mad1 loss, including the time delay between sisters losing Mad1, the motion and position of sisters as they lose Mad1, and the orientation of the sister pair relative to the spindle around Mad1 loss. Fig. S2 shows images of Mad1 loss in monopolar and Hec1-9A cells and quantifies K–K distance in these cells. Fig. S3 shows immunofluorescence images of endogenous Mad2 localization to lateral attachments under tension (recapitulating EYFP-Mad1 localization in live cells) and dynamics of SKAP kinetochore recruitment during Mad1 loss. Video 1 shows an example trajectory of Mad1 loss on both kinetochores in a pair. Video 2 shows an example of Mad1 loss in a monopolar spindle. Video 3 provides an up-close view of a kinetochore pair as it loses Mad1 in order to illustrate centromere tension changes. Video 4 illustrates lateral microtubule attachment at a Mad1-positive kinetochore under persistent tension. Video 5 demonstrates that Mad1 levels are stable at CenpE-rigored (GSK-923295 treated) laterally attached kinetochores that remain stuck away from the metaphase plate. Video 6 shows how Mad1 leaves rapidly after end-on microtubule attachment begins.

Acknowledgments

We thank Jagesh Shah for EYFP-Mad1 PtK2 cells, Michael Davidson for the mCherry–α-tubulin and mRuby2 constructs, Aaron Straight for the mCherry-CenpC construct, Jennifer DeLuca for the Hec1-9A–EGFP construct, Jennifer DeLuca and Jeanne Mick for the rat kangaroo Mad2 antibody, Iain Cheeseman for the SKAP-ΔEB-tdTomato construct, Xiaohu Wan for MATLAB SpeckleTracker, Kurt Thorn for microscopy and image analysis advice, Sue Biggins, Arshad Desai and Ted Salmon for discussions, and David Morgan, Fred Chang, and the Dumont laboratory for discussions and critical reading of the manuscript.

This work was funded by National Institutes of Health grant DP2GM119177 (to S. Dumont), the Rita Allen Foundation and Searle Scholars' Program (to S. Dumont), and a National Science Foundation Graduate Research Fellowship (to J. Kuhn) and the University of California, San Francisco, Moritz Heyman Discovery Fellowship (to J. Kuhn).

The authors declare no competing financial interests.

Author contributions: J. Kuhn performed experiments and analyzed the data. J. Kuhn and S. Dumont conceived the project, designed experiments, and wrote the manuscript.

Submitted: 23 November 2016
Revised: 30 March 2017
Accepted: 26 April 2017

References

Aravamudhan, P., A.A. Goldfarb, and A.P. Joglekar. 2015. The kinetochore encodes a mechanical switch to disrupt spindle assembly checkpoint signalling. *Nat. Cell Biol.* 17:868–879. http://dx.doi.org/10.1038/ncb3179

Cane, S., A.A. Ye, S.J. Luks-Morgan, and T.J. Maresca. 2013. Elevated polar ejection forces stabilize kinetochore–microtubule attachments. *J. Cell Biol.* 200:203–218. http://dx.doi.org/10.1083/jcb.201211119

Cheeseman, I.M., and A. Desai. 2008. Molecular architecture of the kinetochore–microtubule interface. *Nat. Rev. Mol. Cell Biol.* 9:33–46. http://dx.doi.org/10.1038/nrm2310

Collin, P., O. Nashchekina, R. Walker, and J. Pines. 2013. The spindle assembly checkpoint works like a rheostat rather than a toggle switch. *Nat. Cell Biol.* 15:1378–1385. http://dx.doi.org/10.1038/ncb2855

Dick, A.E., and D.W. Gerlich. 2013. Kinetic framework of spindle assembly checkpoint signalling. *Nat. Cell Biol.* 15:1370–1377. http://dx.doi.org/10.1038/ncb2842

Drpic, D., A.J. Pereira, M. Barisic, T.J. Maresca, and H. Maiato. 2015. Polar ejection forces promote the conversion from lateral to end-on kinetochore-microtubule attachments on mono-oriented chromosomes. *Cell Reports.* 13:460–468. http://dx.doi.org/10.1016/j.celrep.2015.08.008

Elting, M.W., C.L. Hueschen, D.B. Udy, and S. Dumont. 2014. Force on spindle microtubule minus ends moves chromosomes. *J. Cell Biol.* 206:245–256. http://dx.doi.org/10.1083/jcb.201401091

Etemad, B., and G.J. Kops. 2016. Attachment issues: kinetochore transformations and spindle checkpoint silencing. *Curr. Opin. Cell Biol.* 39:101–108. http://dx.doi.org/10.1016/j.ceb.2016.02.016

Etemad, B., T.E. Kuijt, and G.J. Kops. 2015. Kinetochore–microtubule attachment is sufficient to satisfy the human spindle assembly checkpoint. *Nat. Commun.* 6:8987. http://dx.doi.org/10.1038/ncomms9987

Foley, E.A., and T.M. Kapoor. 2013. Microtubule attachment and spindle assembly checkpoint signalling at the kinetochore. *Nat. Rev. Mol. Cell Biol.* 14:25–37. http://dx.doi.org/10.1038/nrm3494

Gassmann, R., A.J. Holland, D. Varma, X. Wan, F. Civril, D.W. Cleveland, K. Oegema, E.D. Salmon, and A. Desai. 2010. Removal of Spindly from microtubule-attached kinetochores controls spindle checkpoint silencing in human cells. *Genes Dev.* 24:957–971. http://dx.doi.org/10.1101/gad.1886810

Gorbsky, G.J., and W.A. Ricketts. 1993. Differential expression of a phosphoepitope at the kinetochores of moving chromosomes. *J. Cell Biol.* 122:1311–1321. http://dx.doi.org/10.1083/jcb.122.6.1311

Guimaraes, G.J., Y. Dong, B.F. McEwen, and J.G. Deluca. 2008. Kinetochore-microtubule attachment relies on the disordered N-terminal tail domain of Hec1. *Curr. Biol.* 18:1778–1784. http://dx.doi.org/10.1016/j.cub.2008.08.012

Heinrich, S., E.M. Geissen, J. Kamenz, S. Trautmann, C. Widmer, P. Drewe, M. Knop, N. Radde, J. Hasenauer, and S. Hauf. 2013. Determinants of robustness in spindle assembly checkpoint signalling. *Nat. Cell Biol.* 15:1328–1339. http://dx.doi.org/10.1038/ncb2864

Hiruma, Y., C. Sacristan, S.T. Pachis, A. Adamopoulos, T. Kuijt, M. Ubbink, E. von Castelmur, A. Perrakis, and G.J. Kops. 2015. Competition between MPS1 and microtubules at kinetochores regulates spindle checkpoint signaling. *Science.* 348:1264–1267. http://dx.doi.org/10.1126/science.aaa4055

Howell, B.J., D.B. Hoffman, G. Fang, A.W. Murray, and E.D. Salmon. 2000. Visualization of Mad2 dynamics at kinetochores, along spindle fibers, and at spindle poles in living cells. *J. Cell Biol.* 150:1233–1250. http://dx.doi.org/10.1083/jcb.150.6.1233

Howell, B.J., B.F. McEwen, J.C. Canman, D.B. Hoffman, E.M. Farrar, C.L. Rieder, and E.D. Salmon. 2001. Cytoplasmic dynein/dynactin drives kinetochore protein transport to the spindle poles and has a role in mitotic spindle checkpoint inactivation. *J. Cell Biol.* 155:1159–1172. http://dx.doi.org/10.1083/jcb.200105093

Howell, B.J., B. Moree, E.M. Farrar, S. Stewart, G. Fang, and E.D. Salmon. 2004. Spindle checkpoint protein dynamics at kinetochores in living cells. *Curr. Biol.* 14:953–964. http://dx.doi.org/10.1016/j.cub.2004.05.053

Ji, Z., H. Gao, and H. Yu. 2015. Kinetochore attachment sensed by competitive Mps1 and microtubule binding to Ndc80C. *Science.* 348:1260–1264. http://dx.doi.org/10.1126/science.aaa4029

Kalantzaki, M., E. Kitamura, T. Zhang, A. Mino, B. Novák, and T.U. Tanaka. 2015. Kinetochore–microtubule error correction is driven by differentially regulated interaction modes. *Nat. Cell Biol.* 17:421–433. http://dx.doi.org/10.1038/ncb3128

Kapoor, T.M., M.A. Lampson, P. Hergert, L. Cameron, D. Cimini, E.D. Salmon, B.F. McEwen, and A. Khodjakov. 2006. Chromosomes can congress to the metaphase plate before biorientation. *Science.* 311:388–391. http://dx.doi.org/10.1126/science.1122142

Khodjakov, A., and J. Pines. 2010. Centromere tension: a divisive issue. *Nat. Cell Biol.* 12:919–923. http://dx.doi.org/10.1038/ncb1010-919

King, J.M., and R.B. Nicklas. 2000. Tension on chromosomes increases the number of kinetochore microtubules but only within limits. *J. Cell Sci.* 113:3815–3823.

Kops, G.J., and J.V. Shah. 2012. Connecting up and clearing out: how kinetochore attachment silences the spindle assembly checkpoint. *Chromosoma.* 121:509–525. http://dx.doi.org/10.1007/s00412-012-0378-5

Krefman, N.I., D.G. Drubin, and G. Barnes. 2015. Control of the spindle checkpoint by lateral kinetochore attachment and limited Mad1 recruitment. *Mol. Biol. Cell.* 26:2620–2639. http://dx.doi.org/10.1091/mbc.E15-05-0276

London, N., and S. Biggins. 2014a. Mad1 kinetochore recruitment by Mps1-mediated phosphorylation of Bub1 signals the spindle checkpoint. *Genes Dev.* 28:140–152. http://dx.doi.org/10.1101/gad.233700.113

London, N., and S. Biggins. 2014b. Signalling dynamics in the spindle checkpoint response. *Nat. Rev. Mol. Cell Biol.* 15:736–748. http://dx.doi.org/10.1038/nrm3888

Lukinavičius, G., L. Reymond, E. D'Este, A. Masharina, F. Göttfert, H. Ta, A. Güther, M. Fournier, S. Rizzo, H. Waldmann, et al. 2014. Fluorogenic probes for live-cell imaging of the cytoskeleton. *Nat. Methods.* 11:731–733. http://dx.doi.org/10.1038/nmeth.2972

Magidson, V., C.B. O'Connell, J. Lončarek, R. Paul, A. Mogilner, and A. Khodjakov. 2011. The spatial arrangement of chromosomes during prometaphase facilitates spindle assembly. *Cell.* 146:555–567. http://dx.doi.org/10.1016/j.cell.2011.07.012

Magidson, V., R. Paul, N. Yang, J.G. Ault, C.B. O'Connell, I. Tikhonenko, B.F. McEwen, A. Mogilner, and A. Khodjakov. 2015. Adaptive changes in the kinetochore architecture facilitate proper spindle assembly. *Nat. Cell Biol.* 17:1134–1144. http://dx.doi.org/10.1038/ncb3223

Magidson, V., J. He, J.G. Ault, C.B. O'Connell, N. Yang, I. Tikhonenko, B.F. McEwen, H. Sui, and A. Khodjakov. 2016. Unattached kinetochores rather than intrakinetochore tension arrest mitosis in taxol-treated cells. *J. Cell Biol.* 212:307–319. http://dx.doi.org/10.1083/jcb.201412139

Maldonado, M., and T.M. Kapoor. 2011. Constitutive Mad1 targeting to kinetochores uncouples checkpoint signalling from chromosome biorientation. *Nat. Cell Biol.* 13:475–482. http://dx.doi.org/10.1038/ncb2223

Maresca, T.J., and E.D. Salmon. 2009. Intrakinetochore stretch is associated with changes in kinetochore phosphorylation and spindle assembly checkpoint activity. *J. Cell Biol.* 184:373–381. http://dx.doi.org/10.1083/jcb.200808130

Matson, D.R., and P.T. Stukenberg. 2014. CENP-I and Aurora B act as a molecular switch that ties RZZ/Mad1 recruitment to kinetochore attachment status. *J. Cell Biol.* 205:541–554. http://dx.doi.org/10.1083/jcb.201307137

McEwen, B.F., A.B. Heagle, G.O. Cassels, K.F. Buttle, and C.L. Rieder. 1997. Kinetochore fiber maturation in PtK1 cells and its implications for the mechanisms of chromosome congression and anaphase onset. *J. Cell Biol.* 137:1567–1580. http://dx.doi.org/10.1083/jcb.137.7.1567

McIntosh, J.R. 1991. Structural and mechanical control of mitotic progression. *Cold Sprin. Harb. Symp. Quant. Biol.* 56:613–619. http://dx.doi.org/10.1101/SQB.1991.056.01.070

Musacchio, A., and E.D. Salmon. 2007. The spindle-assembly checkpoint in space and time. *Nat. Rev. Mol. Cell Biol.* 8:379–393. http://dx.doi.org/10.1038/nrm2163

Nezi, L., and A. Musacchio. 2009. Sister chromatid tension and the spindle assembly checkpoint. *Curr. Opin. Cell Biol.* 21:785–795. http://dx.doi.org/10.1016/j.ceb.2009.09.007

Nicklas, R.B., J.C. Waters, E.D. Salmon, and S.C. Ward. 2001. Checkpoint signals in grasshopper meiosis are sensitive to microtubule attachment, but tension is still essential. *J. Cell Sci.* 114:4173–4183.

Nijenhuis, W., G. Vallardi, A. Teixeira, G.J. Kops, and A.T. Saurin. 2014. Negative feedback at kinetochores underlies a responsive spindle checkpoint signal. *Nat. Cell Biol.* 16:1257–1264. http://dx.doi.org/10.1038/ncb3065

O'Connell, C.B., J. Loncarek, P. Hergert, A. Kourtidis, D.S. Conklin, and A. Khodjakov. 2008. The spindle assembly checkpoint is satisfied in the absence of interkinetochore tension during mitosis with unreplicated genomes. *J. Cell Biol.* 183:29–36. http://dx.doi.org/10.1083/jcb.200801038

Pinsky, B.A., and S. Biggins. 2005. The spindle checkpoint: tension versus attachment. *Trends Cell Biol.* 15:486–493. http://dx.doi.org/10.1016/j.tcb.2005.07.005

Rieder, C.L., R.W. Cole, A. Khodjakov, and G. Sluder. 1995. The checkpoint delaying anaphase in response to chromosome monoorientation is mediated by an inhibitory signal produced by unattached kinetochores. *J. Cell Biol.* 130:941–948. http://dx.doi.org/10.1083/jcb.130.4.941

Schmidt, J.C., T. Kiyomitsu, T. Hori, C.B. Backer, T. Fukagawa, and I.M. Cheeseman. 2010. Aurora B kinase controls the targeting of the Astrin–SKAP complex to bioriented kinetochores. *J. Cell Biol.* 191:269–280. http://dx.doi.org/10.1083/jcb.201006129

Shah, J.V., E. Botvinick, Z. Bonday, F. Furnari, M. Berns, and D.W. Cleveland. 2004. Dynamics of centromere and kinetochore proteins; Implications for checkpoint signaling and silencing. *Curr. Biol.* 14:942–952.

Shimogawa, M.M., M.M. Wargacki, E.G. Muller, and T.N. Davis. 2010. Laterally attached kinetochores recruit the checkpoint protein Bub1, but satisfy the spindle checkpoint. *Cell Cycle.* 9:3619–3628. http://dx.doi.org/10.4161/cc.9.17.12907

Shrestha, R.L., and V.M. Draviam. 2013. Lateral to end-on conversion of chromosome-microtubule attachment requires kinesins CENP-E and MCAK. *Curr. Biol.* 23:1514–1526. http://dx.doi.org/10.1016/j.cub.2013.06.040

Smith, C.A., A.D. McAinsh, and N.J. Burroughs. 2016. Human kinetochores are swivel joints that mediate microtubule attachments. *eLife.* 5:e16159. http://dx.doi.org/10.7554/eLife.16159

Tauchman, E.C., F.J. Boehm, and J.G. DeLuca. 2015. Stable kinetochore–microtubule attachment is sufficient to silence the spindle assembly checkpoint in human cells. *Nat. Commun.* 6:10036. http://dx.doi.org/10.1038/ncomms10036

Uchida, K.S., K. Takagaki, K. Kumada, Y. Hirayama, T. Noda, and T. Hirota. 2009. Kinetochore stretching inactivates the spindle assembly checkpoint. *J. Cell Biol.* 184:383–390. http://dx.doi.org/10.1083/jcb.200811028

Wan, X., D. Cimini, L.A. Cameron, and E.D. Salmon. 2012. The coupling between sister kinetochore directional instability and oscillations in centromere stretch in metaphase PtK1 cells. *Mol. Biol. Cell.* 23:1035–1046. http://dx.doi.org/10.1091/mbc.E11-09-0767

Wood, K.W., L. Lad, L. Luo, X. Qian, S.D. Knight, N. Nevins, K. Brejc, D. Sutton, A.G. Gilmartin, P.R. Chua, et al. 2010. Antitumor activity of an allosteric inhibitor of centromere-associated protein-E. *Proc. Natl. Acad. Sci. USA.* 107:5839–5844. http://dx.doi.org/10.1073/pnas.0915068107

Zaytsev, A.V., L.J. Sundin, K.F. DeLuca, E.L. Grishchuk, and J.G. DeLuca. 2014. Accurate phosphoregulation of kinetochore-microtubule affinity requires unconstrained molecular interactions. *J. Cell Biol.* 206:45–59. http://dx.doi.org/10.1083/jcb.201312107